remote sensing

MDPI

Article

A Study on Integration of Topographic Clustering and Physical Constraints for Flood Propagation Simulation

Xu Zhang [1,2,3], Xiaotao Li [1,2,3,*], Yingwei Sun [1,2,3], Qiaomei Su [4], Shifan Yuan [5], Mei Yang [6], Qianfang Lou [6] and Bingyuan Chen [1,2,3]

[1] State Key Laboratory of Simulation and Regulation of Water Cycle in River Basin, China Institute of Water Resources and Hydropower Research, Beijing 100038, China; zhangx@edu.iwhr.com (X.Z.); sunyw@iwhr.com (Y.S.); chenbingyuan@edu.iwhr.com (B.C.)
[2] Remote Sensing Technology Application Center, Ministry of Water Resources, Beijing 100038, China
[3] Engineering Technology Research Center for Flood Control and Drought Relief, Ministry of Water Resources, Beijing 100038, China
[4] College of Geological and Surveying Engineering, Taiyuan University of Technology, Taiyuan 030024, China; suqiaomei@tyut.edu.cn
[5] Power China Kunming Engineering Corporation Limited, Kunming 650051, China; 18834377298@163.com
[6] College of Water Conservancy Science and Engineering, Taiyuan University of Technology, Taiyuan 030024, China; yangmei@tyut.edu.cn (M.Y.); 2024520890@link.tyut.edu.cn (Q.L.)
* Correspondence: lixt@iwhr.com

Highlights

What are the main findings?

- A terrain clustering strategy based on TSLIC is introduced for flood simulation, enabling efficient representation of micro-topographic features while significantly reducing computational units.
- A simplified flood evolution model constrained by remote sensing-derived propagation characteristics is developed, improving temporal realism compared with traditional static inundation methods.

What are the implications of the main findings?

- The proposed framework improves computational efficiency by more than 60% while maintaining water level and inundation extent errors within 10%, supporting rapid flood simulation under emergency conditions.
- The method demonstrates the potential of combining high-resolution terrain data and remote sensing-derived flood dynamics to support flood regulation and decision-making in flood storage–detention basins.

Abstract

Global climate change is increasing extreme rainfall events, and severe floods are becoming more frequent. Flood storage and detention basins (FSDBs) are an important part of the flood control system in China. They play a key role in regional flood emergency response and regulation. Therefore, accurate simulation of flood evolution after the activation of FSDBs is urgently needed. This study proposes a high-accuracy flood evolution simulation method that combines terrain clustering and physical propagation constraints. We first build a 2 m resolution digital elevation model (DEM) using GF-7 stereo imagery and laser altimetry data. We then introduce an improved superpixel segmentation algorithm (TSLIC). This method reduces the number of computational units while preserving key micro-topographic features. It groups high-resolution grids into terrain units with similar elevation characteristics and continuous spatial structure. Based on these terrain units, we develop a flood evolution model called RS-CFPM. The model combines flow velocity estimated from the Manning equation with flood propagation speed derived from radar

Check for updates

Academic Editor: Donglian Sun

Received: 14 January 2026
Revised: 18 February 2026
Accepted: 4 March 2026
Published: 13 March 2026

Copyright: © 2026 by the authors. Licensee MDPI, Basel, Switzerland. This article is an open access article distributed under the terms and conditions of the Creative Commons Attribution (CC BY) license.

remote sensing. It uses a water balance framework and includes a propagation time delay constraint. This design helps overcome the limitation of traditional static inundation methods that ignore flood travel time. We apply the proposed method to simulate the flood inundation process during the "23·7" extreme basin-scale flood event in the Haihe River Basin. Comparison with multi-temporal radar observations shows that the errors of simulated water level and inundation extent in the Dongdian FSDB are both within 10%. The computational efficiency is also improved by more than 60% compared with traditional methods. This study provides a new approach for rapid and accurate simulation of flood inundation processes in FSDBs under emergency conditions. The method can support flood emergency operation and decision-making.

Keywords: flood storage-detention basin (FSDB); flood evolution; TSLIC; water depth; inundation extent

1. Introduction

Flood disasters are among the most destructive natural hazards worldwide and pose serious threats to socioeconomic development, ecological stability, and human life and property [1–4]. With the intensification of global climate change and the increasing occurrence of extreme weather events, both the intensity and frequency of heavy rainfall and flood events have continued to rise, which further increases the urgency of flood control and disaster reduction [5–7]. In China, many middle and lower reaches of river basins are located in low-lying plains with dense populations and developed economies, making these areas highly vulnerable to flood disasters [8,9]. Flood storage–detention basins (FSDBs) are an important engineering measure in flood control systems. By storing and diverting excess floodwater in a planned manner, FSDBs can effectively reduce flood peaks and lower downstream water levels. They therefore play a critical role in protecting major cities and key infrastructure and have irreplaceable strategic importance in flood risk management [10–12].

During flood emergency response, rapid and accurate simulation of flood evolution within flood storage–detention basins (FSDBs) is critical, as it directly affects the reliability of regulation decisions and the effectiveness of disaster mitigation measures [13]. To simulate inundation extent and water depth distribution, several approaches are commonly used, including ground-based monitoring [14], hydrodynamic modeling [15–18], and GIS-based inundation simulation [19]. Ground-based monitoring can provide high-accuracy water level observations. However, its spatial coverage is limited. It is difficult to continuously capture large-scale inundation dynamics, which restricts its use in regional flood evolution modelling. Hydrodynamic models based on physical mechanisms solve the shallow water equations and consider terrain, roughness, inflow boundary conditions, and flow dynamics. These models can achieve high simulation accuracy [20–22]. However, they usually require detailed terrain and hydrological data. They also need complex parameter calibration and high computational resources. As a result, they are difficult to apply in large-scale areas or rapid emergency response scenarios [23]. To improve computational efficiency, some studies use GIS-based inundation models, such as the Bathtub model and cellular automata (CA) models. These methods estimate inundation extent by gradually raising water levels on DEMs or by applying local expansion rules [24–26]. They are suitable for large areas where detailed hydrological data are lacking or where rapid assessment is needed. However, these methods ignore flood travel time, flow velocity variation, and momentum effects [27–31]. Therefore, they cannot fully represent real flood evolution

processes. This limitation is especially obvious during dynamic rising stages, where inundation timing and extent may be misestimated.

In summary, existing flood evolution simulation methods still face a clear trade-off between accuracy and computational efficiency. Because of this, they often cannot meet both accuracy and timeliness requirements under emergency flood conditions. To address this problem, this study proposes a flood evolution simulation method for flood storage and detention basins that combines terrain clustering and physical propagation constraints. The method does not aim to replace full hydrodynamic models. Instead, it serves as a high-efficiency tool for rapid emergency decision support in plain flood detention areas. To improve computational efficiency when using high-resolution DEMs over large areas, we introduce a DEM-based superpixel segmentation algorithm [32–35]. This method groups grid cells into terrain units with similar elevation characteristics and continuous spatial structure. It preserves key micro-topographic controls and overall spatial patterns while reducing the number of computational units. As a result, the method lowers computational complexity while maintaining terrain representation ability. At the same time, traditional static inundation models often ignore flood travel time and dynamic evolution processes. Full hydrodynamic models, however, usually require high computational cost. To bridge this gap, we develop the RS-CFPM model within a water balance framework. The model introduces a propagation time constraint and combines theoretical flow velocity from the Manning equation with flood propagation speed derived from radar remote sensing. This design enables the model to capture the temporal characteristics of flood evolution while maintaining high computational efficiency and improving physical consistency.

2. Methods

2.1. Overall Technical Workflow of the Study

This study aims to develop a remote sensing-driven rapid flood evolution simulation framework for flood storage–detention basins (FSDBs). By fully using high-resolution remote sensing terrain data and flood monitoring information, the framework enables dynamic simulation of flood inundation processes under emergency conditions. The overall workflow is shown in Figure 1 and includes the following key steps.

(1) Terrain clustering based on DEM data. First, a high-accuracy digital elevation model (DEM) is constructed using GF-7 stereo imagery and laser altimetry data to represent terrain variation within the FSDB accurately [36]. A terrain-based superpixel clustering method, Terrain-based Simple Linear Iterative Clustering (TSLIC), is then applied to spatially aggregate DEM grids into a set of terrain units with similar elevation characteristics and spatial continuity. This approach preserves the main terrain control features while significantly reducing terrain complexity and computational cost.

(2) Flood evolution simulation constrained by remote sensing data. A flood evolution simulation method that couples water balance with propagation time constraints, referred to as the Remote Sensing–Constrained Flood Propagation Model (RS-CFPM), is developed. The model uses the clustered terrain units as basic computational elements and applies water balance as the core principle. During time stepping, flood inundation extent and water level are updated simultaneously, while propagation time delays are introduced to constrain flood spreading speed and represent the temporal characteristics of flood propagation under real terrain conditions. Multi-temporal radar remote sensing-derived inundation extent and water level information are used for quantitative validation and analysis of the simulation results.

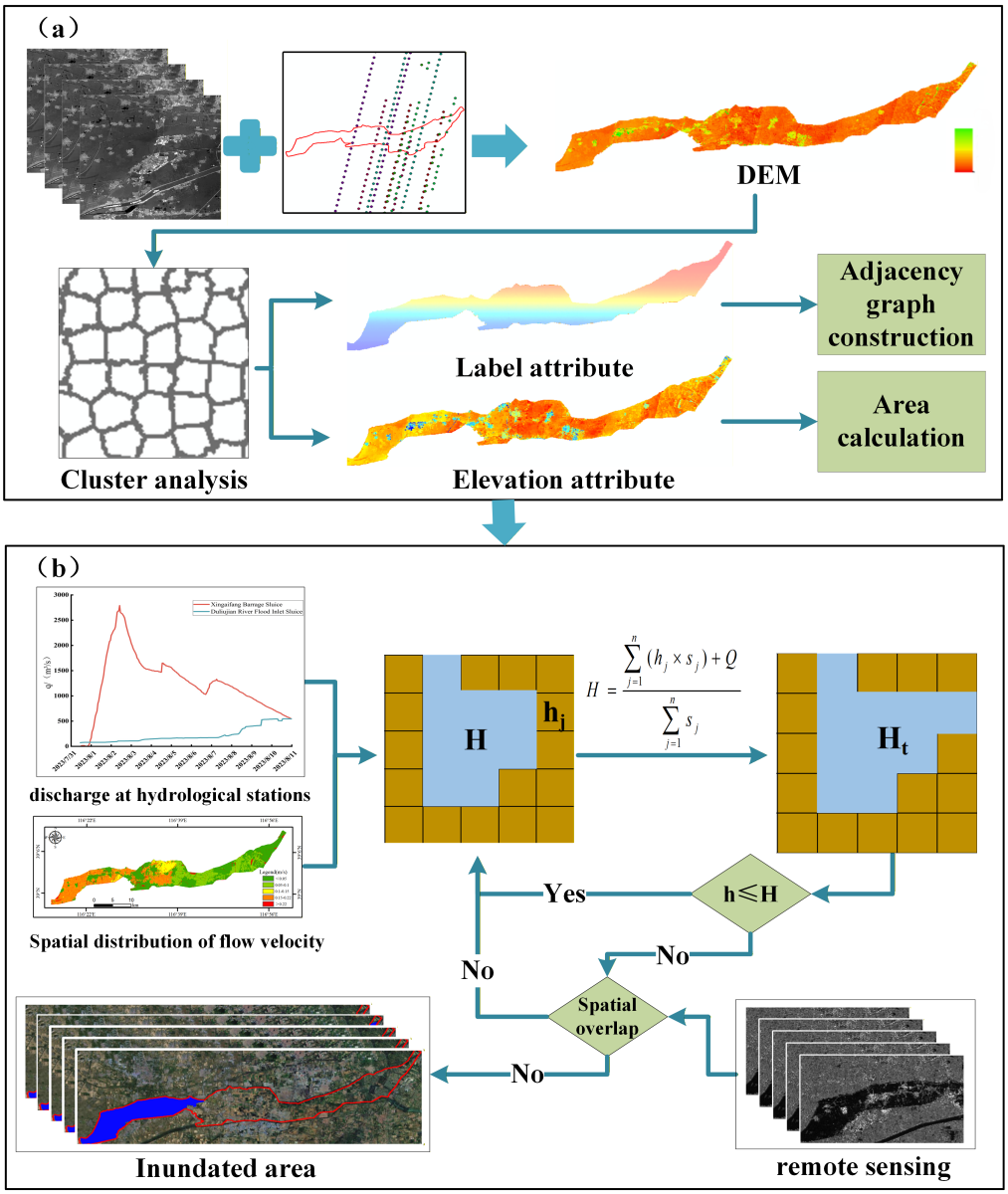


Figure 1. Flood Dynamic Simulation Technology Framework: (**a**) Terrain-based Simple Linear Iterative Clustering, (**b**) Remote Sensing–Constrained Flood Propagation Model. In (**b**) the blue area represents the inundated region, and the yellow area represents the non-inundated region. H is the current average water level, and h_j is the elevation of a terrain unit. If the unit is inundated, H_t represents the newly calculated water level.

2.2. Terrain Clustering Method Based on DEM Data

High-resolution DEMs derived from remote sensing can accurately represent micro-topographic variations within flood storage–detention basins (FSDBs). These DEMs are one of the most important data sources for flood evolution simulation. In relatively flat FSDBs, elevation differences between neighboring grid cells are usually small, and these cells often show similar responses during flood inundation. Therefore, when DEM grid cells are directly used as computational units for flood simulation, the number of units becomes very large and computational efficiency decreases significantly, while the improvement in simulation accuracy remains limited.

To address this issue, this study introduces a terrain clustering method based on elevation characteristics, referred to as Terrain-based Simple Linear Iterative Clustering

(TSLIC). The method spatially aggregates DEM grid cells to construct terrain units for flood simulation. TSLIC is derived from the Simple Linear Iterative Clustering algorithm [37], in which DEM elevation values replace the color features used in traditional image segmentation. This allows the algorithm to identify grid cells that are both spatially adjacent and similar in elevation and to cluster them into terrain units with consistent elevation characteristics and spatial continuity.

During the TSLIC clustering process, each terrain unit represents a continuous area with relatively uniform elevation characteristics. In the subsequent flood evolution simulation, the average elevation and corresponding area of each terrain unit are used as model parameters. This approach preserves the spatial pattern of flood propagation controlled by terrain variation, while it significantly reduces the number of computational units and improves overall simulation efficiency. The improved distance calculation formula is given as follows:

$$d_t = \sqrt{(h_j - h_i)^2} \tag{1}$$

$$d_s = \sqrt{(x_j - x_i)^2 + (y_j - y_i)^2} \tag{2}$$

$$D = \sqrt{d_t^2 + \left(\frac{m}{l}\right)^2 d_s^2} \tag{3}$$

where h_i and h_j is elevations of pixel i and seed point j, respectively; d_t represents the Euclidean distance in the DEM elevation space; x_i and y_i are spatial coordinates of pixel i in the two-dimensional plane; x_j and y_j are spatial coordinates of seed point j; d_s denotes the Euclidean distance in the spatial (x, y) domain; m is the compactness factor; l denotes the distance between seed points; and D is the total distance between a pixel and a seed point.

2.3. Flood Evolution Method Constrained by Remote Sensing

In flood emergency simulation for flood storage–detention basins (FSDBs), flood evolution is controlled not only by terrain elevation but also by flood propagation time effects. Traditional inundation simulation methods based on a static water level assumption, such as the Bathtub Model, usually ignore the physical time required for flood propagation over real terrain. As a result, these methods tend to overestimate inundation extent during flood evolution simulation.

To represent flood evolution more realistically while avoiding the high computational cost of solving full hydrodynamic equations, this study develops a simplified flood evolution simulation method that couples water balance with propagation time constraints, referred to as the Remote Sensing–Constrained Flood Propagation Model (RS-CFPM). The model uses TSLIC terrain units, rather than individual DEM grid cells, as the basic computational elements and advances flood evolution using discrete time steps. At each time step, the model first accumulates inflow over time to obtain the cumulative flood volume at the current moment. Next, the initial inundation mask is overlaid on the DEM, and the elevation and area of terrain units within the inundated region are extracted. The model assumes that the water surface within the inundated area is approximately level. Based on this assumption, it estimates the average water level using the cumulative flood volume, the area-weighted elevation, and the total inundated area. Finally, the model compares the calculated water level with the elevation of each terrain unit. It then determines whether each unit is inundated and updates the inundation extent accordingly. The equations are expressed as follows:

$$Q = \sum_{i=1}^{n} q_i \cdot t \tag{4}$$

$$H = \frac{\sum_{j=1}^{n}(h_j \cdot s_j) + Q}{\sum_{j=1}^{n} s_j} \tag{5}$$

Among these, Q represents the cumulative flood volume, q denotes the runoff inflow, H is the water level, h is the elevation of the superpixel, s is the area of the superpixel, i indicates the time step, and j represents the superpixel label. The total inundated area is defined as the sum of the areas s of all superpixels whose elevation values are lower than the current water level H.

In this study, the model first calculates the physical inundation extent based on the comparison between water level and terrain elevation (areas where $H > h_j$). The study focuses on flood emergency applications. In real emergency management, residential areas may not be directly covered by water but can still be surrounded by floodwater, cut off from transportation, or exposed to safety risks. These areas are usually included in inundation impact statistics. Therefore, the terms "inundation extent" and "inundation area" in this study refer to the emergency inundation extent, which combines the physically inundated area with residential areas enclosed by floodwater.

To prevent instantaneous spatial spreading of floodwater, the model further introduces a propagation time constraint to control the propagation speed of floodwater between adjacent terrain units. Flood propagation speed is estimated from two sources. First, the Manning equation is used to calculate flow velocity, which reflects the influence of surface roughness and slope under different terrain conditions. Second, multi-temporal radar remote sensing images are used to extract the actual movement speed of the flood front, which represents flood propagation behavior over real terrain. The model combines these two velocity estimates using a weighted average approach. The resulting velocity is then used to determine the time required for floodwater to propagate between adjacent terrain units. The equations are given as follows:

$$v = \lambda \frac{1}{n} R^{2/3} J^{1/2} + (1 - \lambda) V \tag{6}$$

$$R = A/L \tag{7}$$

where n is the Manning's roughness coefficient, R denotes the hydraulic radius, J represents the hydraulic gradient, λ is the weighting coefficient, V indicates the average flow velocity, A refers to the cross-sectional area, and L is the wetted perimeter.

3. Study Area and Data

3.1. Study Area

The Dongdian flood storage–detention basin (Dongdian FSDB) is located in the Haihe River Basin and lies in the lower reaches of the Daqing River system. It serves as a flood storage and detention area for floodwaters from the northern and southern branches of the Daqing River, as well as runoff from the Qingnan and Qingbei drainage channels. The eastern boundary of the basin is defined by the right levee of the Ziya River. It is bounded to the south by the Qianli Levee, the Gedian Levee, and the right levee of the Ziya River, to the west by Baiyangdian Lake and the Xingaiyang flood diversion channel, and to the north by the Zhongting Levee. The basin covers parts of Bazhou City and Wen'an County in Hebei Province, as well as Jinghai District in Tianjin Municipality (Figure 2). The basin extends approximately 66 km from east to west and 2.5–9 km from north to south. The terrain is higher in the west and lower in the east, with a gentle surface slope ranging from 1/6000 to 1/10,000. Ground elevation ranges from −10 m to −4 m. The total area of the Dongdian FSDB is 378.8 km^2, of which 264.90 km^2 lies in Hebei Province and 113.86 km^2 lies in Tianjin Municipality.

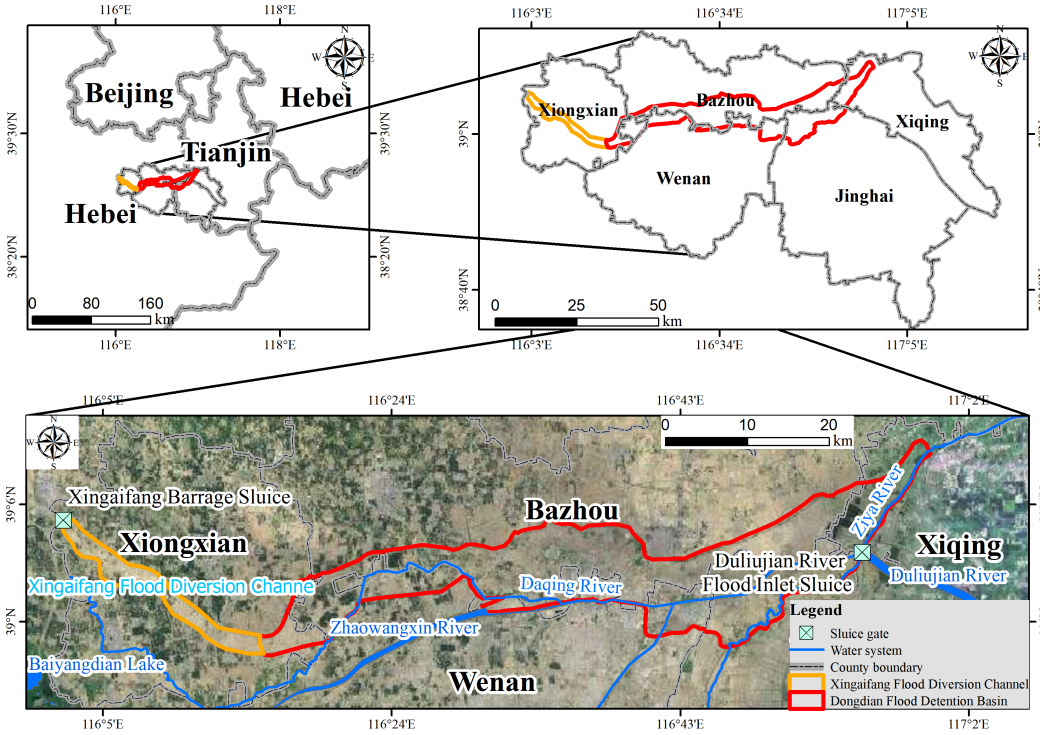


Figure 2. Overview of the study area.

From 28 July to 1 August 2023, the Haihe River Basin experienced the most intense rainfall event since 1963 due to the influence of Typhoon Doksuri. Multiple flood events occurred successively in the Ziya River, Yongding River, and Daqing River systems [38,39]. At 02:00 on 1 August 2023, the Dongdian FSDB was activated. As shown in Figure 3, the flood regulation process in the Dongdian FSDB can be divided into a rising stage (2 August–10 August) and a recession stage (10 August–26 September). The recession stage can be further divided into a natural drainage period (10 August–24 August) and a pumping drainage period (24 August–26 September). In this study, the rising stage of the flood regulation process in the Dongdian FSDB is selected for flood inundation simulation.

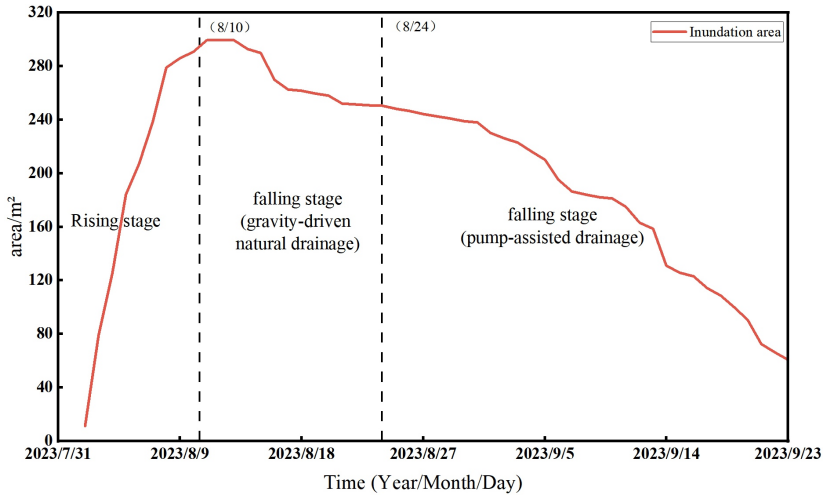


Figure 3. Flood routing.

3.2. Data

3.2.1. Satellite Data

The DEM used in this study was generated from GF-7 satellite DLC stereo imagery and laser altimetry (LSA) products. GF-7 data products were obtained from the China

Centre for Resources Satellite Data and Application (https://data.cresda.cn/). The LSA altimetry products are also provided through the official GF-7 data service platform. The GF-7 satellite adopts an active–passive integrated optical mapping system and is equipped with a dual-line array camera and a laser altimeter. The dual-line array camera can acquire optical remote sensing imagery with a swath width of 20 km, with a forward-looking spatial resolution better than 0.8 m, a backward-looking resolution better than 0.65 m, and a multispectral resolution better than 2.6 m. The laser altimetry system includes a two-beam laser transmitter operating at a frequency of 3 Hz. The laser footprints have an along-track spacing of approximately 2.4 km and a cross-track spacing of about 12.25 km, forming two rows with a total of 16 laser points within a 20 km × 20 km image coverage area [40]. To fully cover the Dongdian FSDB, seven scenes of GF-7 DLC stereo imagery were used for DEM generation, and six scenes of laser altimetry data were used for DEM accuracy assessment. In addition, six scenes of radar remote sensing images acquired during the flood regulation period and covering the Dongdian FSDB were collected. Detailed information on these datasets is summarized in Table 1.

Table 1. Remote sensing and altimetry datasets used in this study.

Serial Number	Data Type	Date	Serial Number	Data Type	Date	Serial Number	Data Type	Date
1	GF7	20 January 2023	8	altimetry data	19 January 2024	15	GF3B	5 August 2023 18:03
2	GF7	23 May 2023	9	altimetry data	16 May 2024	16	GF3B	6 August 2023 06:10
3	GF7	16 July 2023	10	altimetry data	14 July 2024	17	GF3B	7 August 2023 06:20
4	GF7	16 July 2023	11	altimetry data	4 November 2024	18	GF3B	7 August 2023 18:20
5	GF7	14 January 2024	12	altimetry data	9 November 2024	19	GF3C	10 August 2023 17:17
6	GF7	11 May 2024	13	altimetry data	7 January 2025			
7	GF7	7 January 2025	14	HJ2E	3 August 2023 10:41			

3.2.2. Other Data

This study collected discharge data from the Xingaiyang Flood Diversion Channel hydrological station and the Duliujian River inflow gate hydrological station, which are published on the Tianjin Municipal Water Information Release Platform. During the flood regulation period in the Dongdian FSDB, both stations recorded hydrological information at an hourly time interval.

GF-1B satellite data were used to generate a land use map for the Dongdian area. Land cover was classified into six categories: residential areas, roads, cropland, forest land, grassland, and water bodies (Figure 4). Cropland and residential areas are the dominant land use types in the Dongdian FSDB, accounting for approximately 70% and more than 15% of the total area, respectively, while all other land cover types together account for less than 15%.

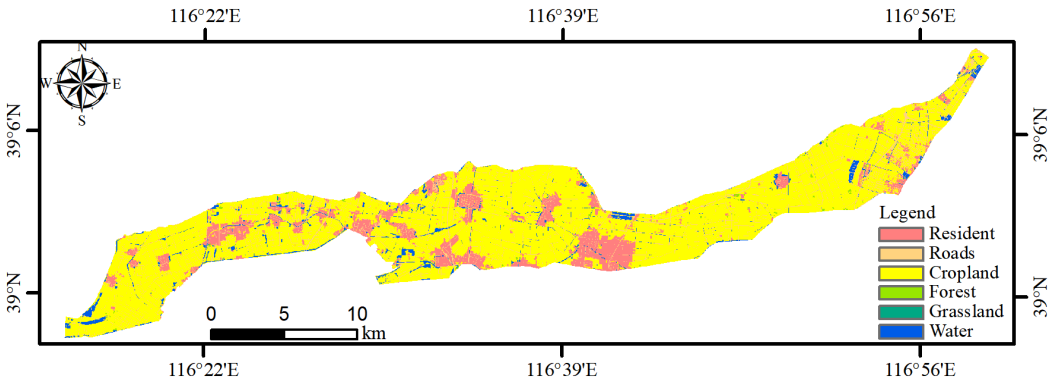


Figure 4. Land use classification in Dongdian Flood Detention Basin.

4. Results

4.1. Analysis of Flood Simulation Results in the FSDB

In this study, forward- and backward-looking images acquired by the dual linear array camera (DLC) onboard the GaoFen-7 (GF-7) satellite were used. Their rational polynomial coefficients (RPCs) were also used. We applied block adjustment to obtain accurate image orientation. Based on the refined orientation parameters, we performed stereo matching on the satellite image pairs; this process generated an initial digital surface model (DSM) with a spatial resolution of 2 m. To derive ground elevation information for flood simulation, we further processed the initial DSM. The required information included elevations of highways, bridges, and residential areas. We applied inverse distance weighting (IDW) interpolation to the relevant regions. Local filtering and masking operations were then performed to remove non-ground objects. Through these steps, the final digital elevation model (DEM) of the Dongdian FSDB was generated, as shown in Figure 5.

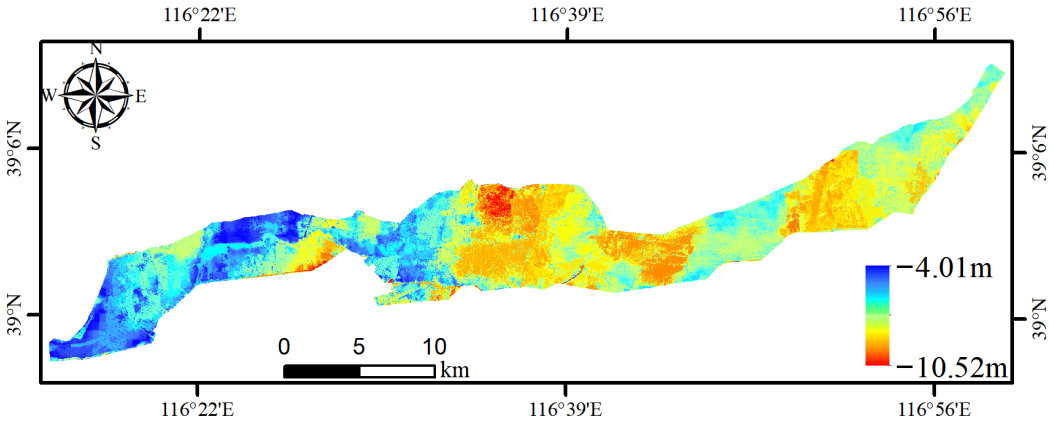


Figure 5. 2m-resolution DEM of Dongdian FSDB.

The original laser altimetry data were strictly filtered; only data points with optimal quality flags were retained, including a location quality flag (Location Flag), variable-gain waveform quality flag (Wave Vgain Flag), and fine-gain waveform quality flag (Wave Fgain Flag) all equal to 1 [40,41]. The filtered data were then spatially clipped using the boundary of the Dongdian study area, resulting in a total of 17 high-quality altimetry points.

DEM elevation values corresponding to the spatial locations of the 17 altimetry points were extracted for accuracy assessment. The results show that the relative elevation errors between the DEM and the altimetry points are all less than 20%, with six points having errors below 10%. In addition, the elevation differences between the DEM and the altimetry points fall within the range of −1 m to 1 m, and 11 points fall within −0.7 m to 0.7 m. As the Dongdian FSDB is characterized by flat terrain, the computed root mean square error (RMSE) of elevation is 0.67 m, which meets the second-order accuracy requirement for flat terrain areas [36]. These results indicate that the generated DEM has satisfactory accuracy.

This study simulated a 7-day flood regulation process from 2 August to 10 August and obtained multi-temporal inundation information, including inundation extent and water level. It should be noted that at 05:00 on 10 August, a rapid rise in water level in the Daqing River caused backflow into the Tanli drainage channel and led to a breach of the right levee. As a result, parts of the right bank of the Daqing River were inundated. The inundation caused by this breach occurred outside the simulation domain and was therefore not included in the figures or analysis presented in this study.

Multi-temporal radar remote sensing images were used to calculate the Synthetic Difference Water Index (SDWI), and a traditional thresholding method (OTSU) was applied to extract water bodies and obtain instantaneous inundation extents during the flood

event. Natural water surfaces were approximated as horizontal planes. For each time step, the inundation extent mask was overlaid on the DEM to extract elevation values along the water boundary. A weighted average of these elevation values was then calculated to estimate the water level corresponding to the inundation extent. It should be noted that the water masks extracted from SAR imagery using the SDWI and OTSU methods represent the physical water surface extent. To ensure consistency with the model output, this study applies the same definition of emergency inundation extent to the remote sensing results. Therefore, residential units that are completely surrounded by water are additionally included in the statistics. These units are incorporated into the calculation of the emergency inundation area. The extracted inundation information is summarized in Table 2.

Table 2. Inundation area and water level derived from remote sensing.

Serial Number	Date	Inundation Area (km^2)	Water Level (m)
1	3 August 2023 10:41	79.47	−5
2	5 August 2023 18:03	184.14	−6.13
3	6 August 2023 06:10	207.21	−5.64
4	7 August 2023 06:20	238.12	−5.85
5	7 August 2023 18:20	256.48	−5.75
6	10 August 2023 17:17	270.49	−5.58

This study achieved hourly simulation of the flood inundation process in the Dongdian FSDB. After validation using six available remote sensing images, the model was further applied to simulate inundation conditions on 4, 8, and 9 August, when no remote sensing observations were available. In addition, inundation area changes from 2 to 5 August were output at 12-hour intervals, resulting in a total of nine inundation snapshots. Figures 6 and 7 clearly illustrate the dynamic evolution of flood inundation in the Dongdian FSDB. It should be noted that Figures 6 and 7 present representative examples of the simulation results.

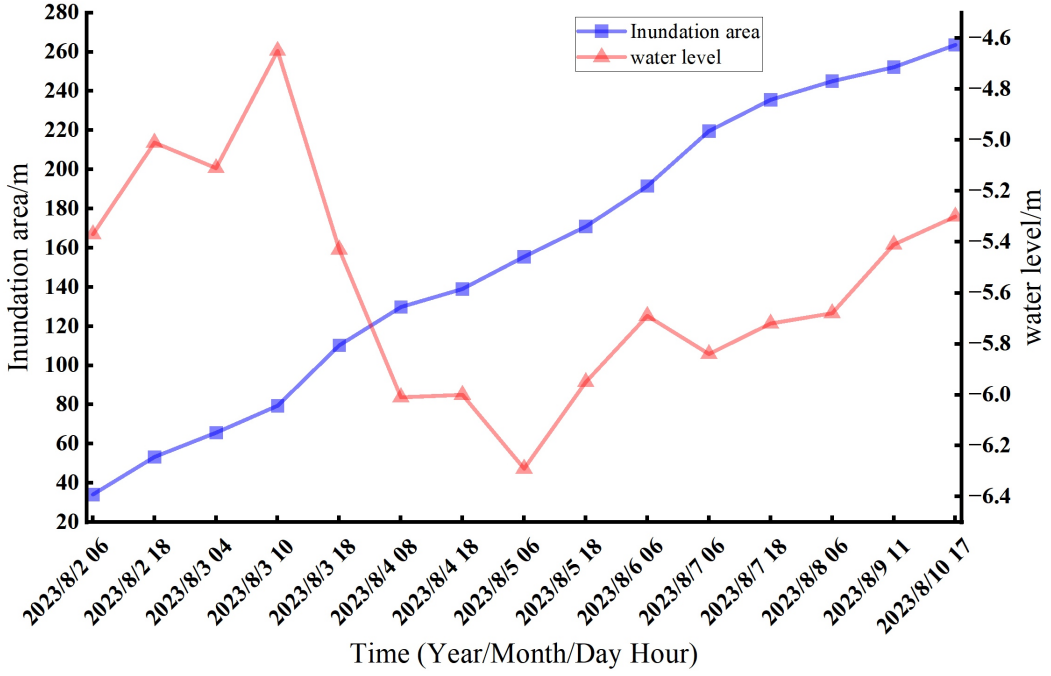


Figure 6. Temporal variations in simulated inundation area and water level.

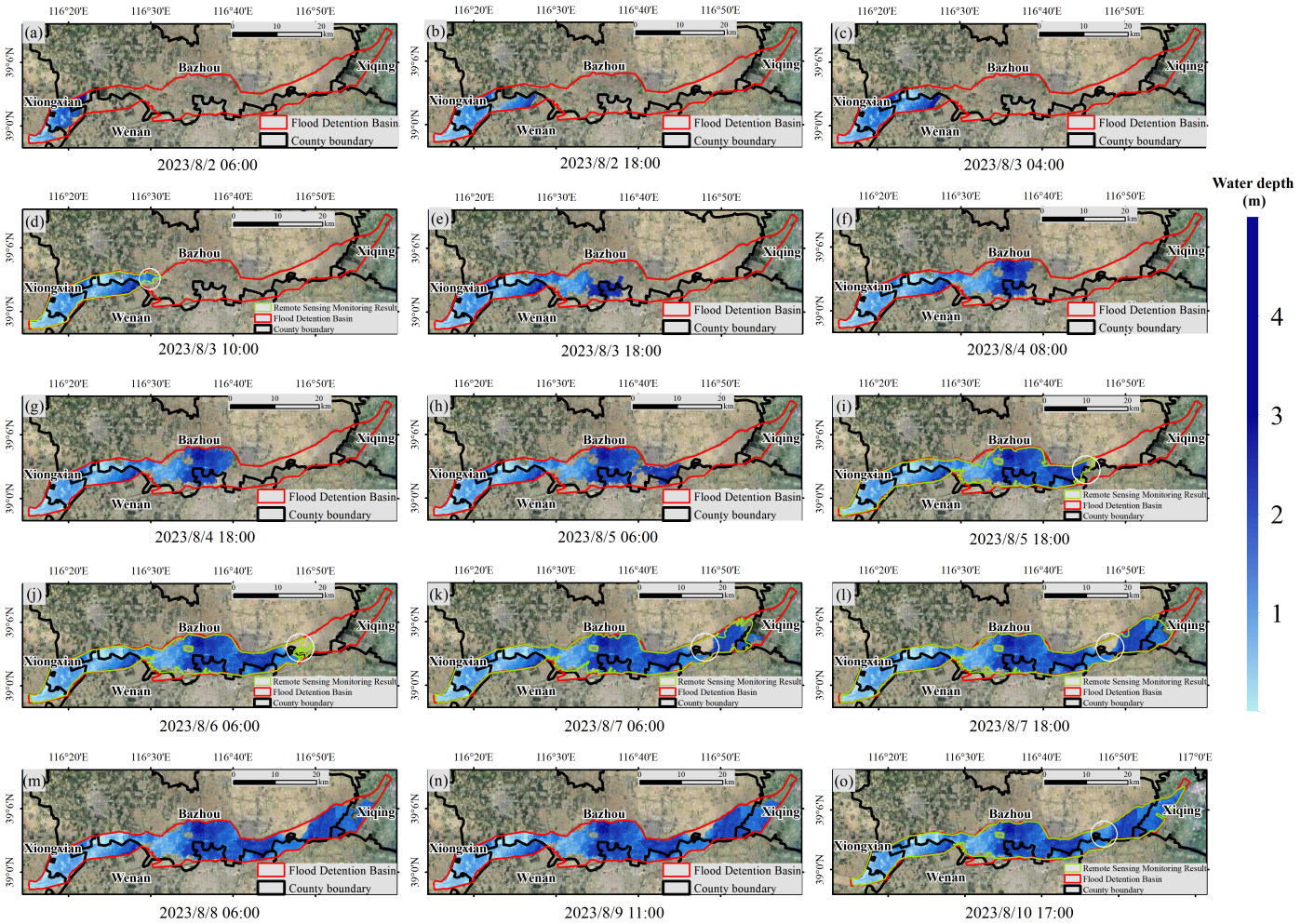


Figure 7. Simulated flood propagation process.

Comparison between the simulated inundation extents and remote sensing observations shows good agreement, with inundation area errors consistently within 10% (Figure 8), which confirms the reliability of the proposed model. The largest area error was observed on 5 August. This error was mainly caused by local elevation errors in the generated DEM. In this area (circled in Figure 7i), abnormally elevated terrain values led to temporary water retention, which slowed flood propagation and delayed inundation. As flood inflow continued to increase (Figure 7j), floodwater overtopped the elevated area at 06:00 on 6 August. Between 06:00 and 18:00 on 7 August, this area was gradually inundated, and it became fully submerged at 17:00 on 10 August. At this point, the Dongdian FSDB reached its maximum inundation area of 263.72 km^2.

Error analysis results show that the differences between simulated water levels and remote sensing observations are all within 10%, and four time steps have water level errors below 5%, indicating good overall simulation performance (Figure 9). The largest water level error was observed on 3 August. This error mainly resulted from data processing. In this area (circled in Figure 7d), residential buildings are dense and highly clustered. During terrain clustering, some small neighboring ground units were incorrectly merged into the "residential area" class, which led to locally increased elevation values. This clustering error caused overestimated terrain elevation in the model input and, therefore, resulted in a higher simulated water level on 3 August compared with the observed value.

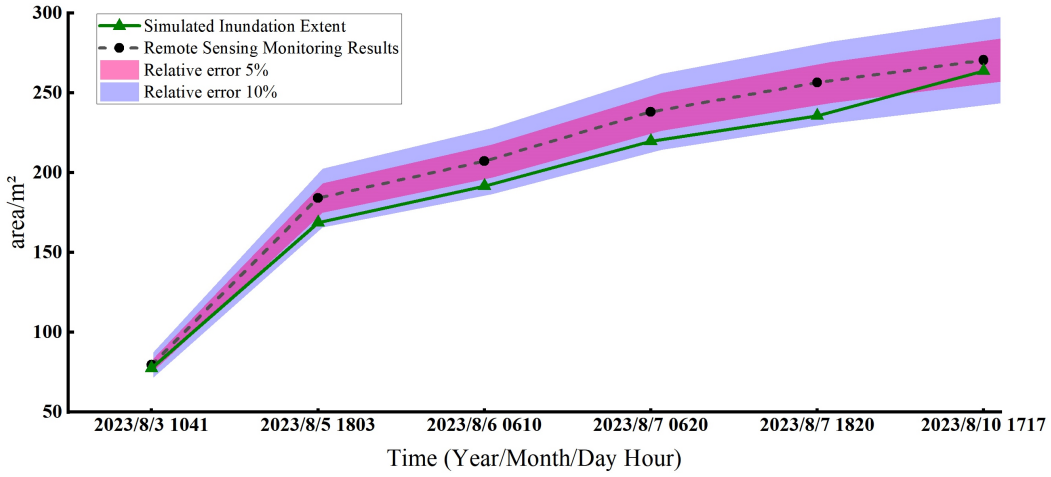


Figure 8. Comparison of Relative Errors between Simulated Inundation Extents and Remote Sensing Monitoring Results.

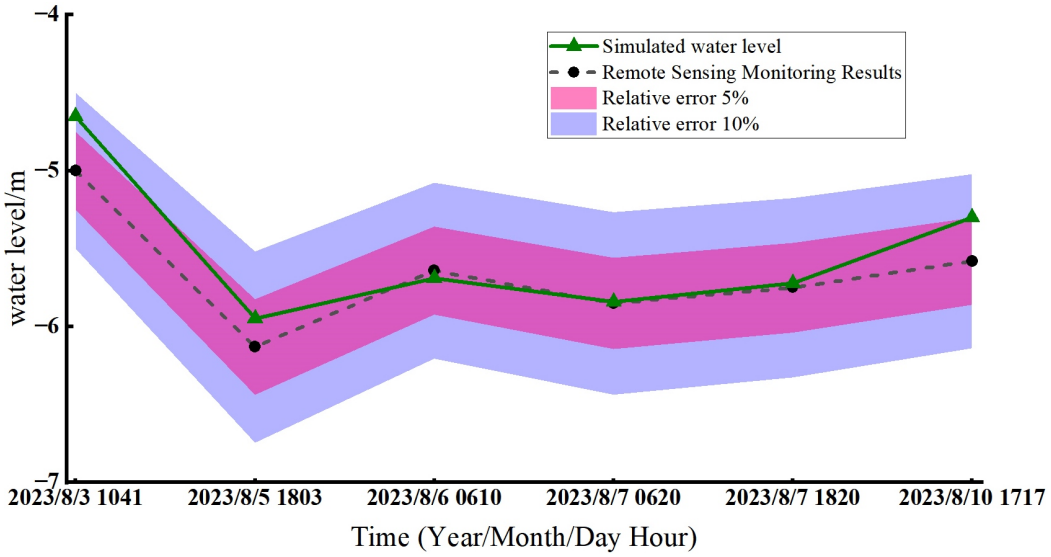


Figure 9. Comparison of Relative Errors between Simulated Water Levels and Remote Sensing Water Levels.

To evaluate the computational efficiency of the proposed RS-CFPM model, runtime tests were conducted by gradually increasing the number of input grid cells while keeping all other input information and time step settings strictly consistent. The efficiency comparison results (Table 3) clearly show that, compared with the traditional Bathtub Model, the proposed model achieves a significant improvement in computational efficiency. In all test scenarios, the runtime of the proposed model was substantially reduced, with efficiency gains exceeding 60%. Further analysis shows that the model runtime increases approximately linearly with the number of grid cells. This indicates that the algorithm has good scalability when applied to large spatial datasets. In the Dongdian FSDB, a complete flood evolution simulation takes less than three minutes. This result demonstrates that the model can achieve minute-level computational response for datasets with tens of millions of grid cells. Therefore, the model can meet the demand for rapid decision support in flood emergency simulations.

Table 3. Computational efficiency comparison of flood simulation models.

Serial Number	Number of Grids	RS-CFPM (s)	Bathtub Mode (s)	Efficiency Improvement
1	9.6×10^6	11.76	38.48	69.44%
2	19.1×10^6	23.05	62.68	63.23%
3	41×10^6	61.34	189.97	67.71%
4	81.1×10^6	127.43	343.11	62.86%

4.2. Analysis of Flood Evolution Methods

4.2.1. Comparison of Terrain Clustering Methods

In the superpixel segmentation algorithm (TSLIC), the number of superpixels N and the compactness factor m have a decisive influence on segmentation results. The compactness factor m is used to balance the weights of spatial distance and elevation features, and its typical value ranges from 1 to 40. When m is too small, segmentation boundaries tend to be irregular. When m is too large, the segmentation result approaches uniform square-shaped units. In contrast, when m is fixed, adjusting N allows for the setting of an appropriate number of superpixels while preserving the integrity of the terrain structure. This helps optimize the computational efficiency of flood simulation. If N is too large, the computational efficiency of the flood simulation decreases. Based on these considerations, the parameters for the study area are set as m = 10 and N = 20,095, with each superpixel typically covering between 5000 and 6000 grid cells (the exact number varies depending on terrain changes). To evaluate the performance of TSLIC segmentation, a traditional elevation-based Partitioning method was applied for comparison. In this method, the DSM was divided and merged using different elevation intervals, with the interval step set to 0.2 m. The results (Figure 10) show that the traditional elevation-based Partitioning method produces fragmented blocks with uneven areas. Flat regions are often merged into large single blocks, while small terrain features with local elevation differences form scattered small patches. In contrast, TSLIC can accurately delineate terrain boundaries and generate compact, spatially connected, and regular terrain units. These results indicate that TSLIC is more suitable for terrain partitioning in flood simulation applications.

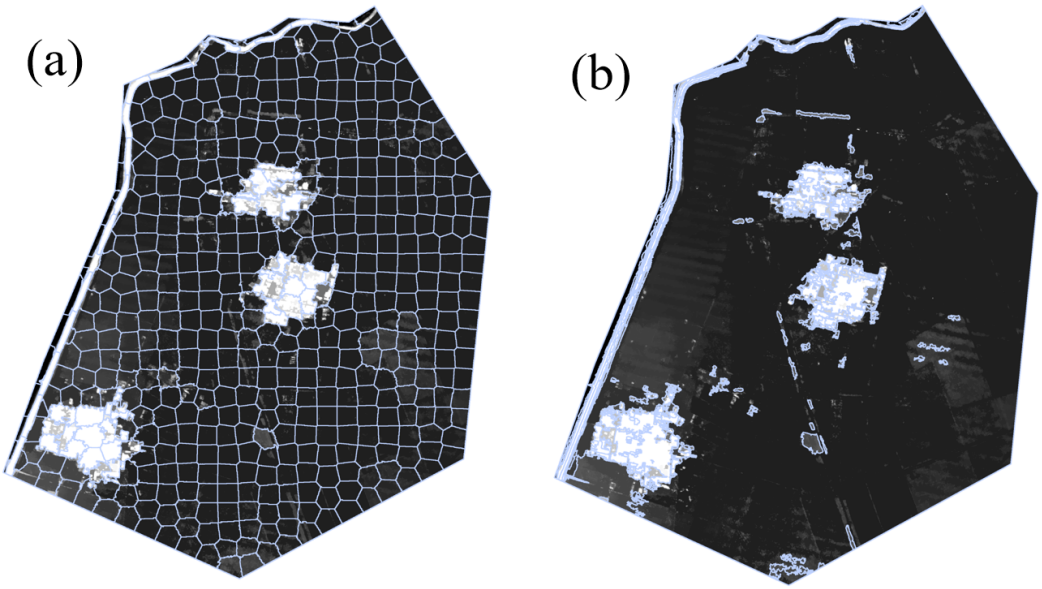


Figure 10. Clustering performance: (**a**) TSLIC; (**b**) elevation-based Partitioning method.

To evaluate the impact of TSLIC-based terrain clustering on flood simulation performance, this study used the TSLIC clustering result and the traditional elevation-based Partitioning method result as two different terrain inputs. Both terrain datasets were simu-

lated using the same RS-CFPM model to obtain dynamic changes in inundation extent. It should be noted that simulations were conducted only for time steps with available remote sensing images, as well as for 4, 8, and 9 August. Figure 11 provides a direct comparison of the inundation dynamics simulated by the two terrain representations.

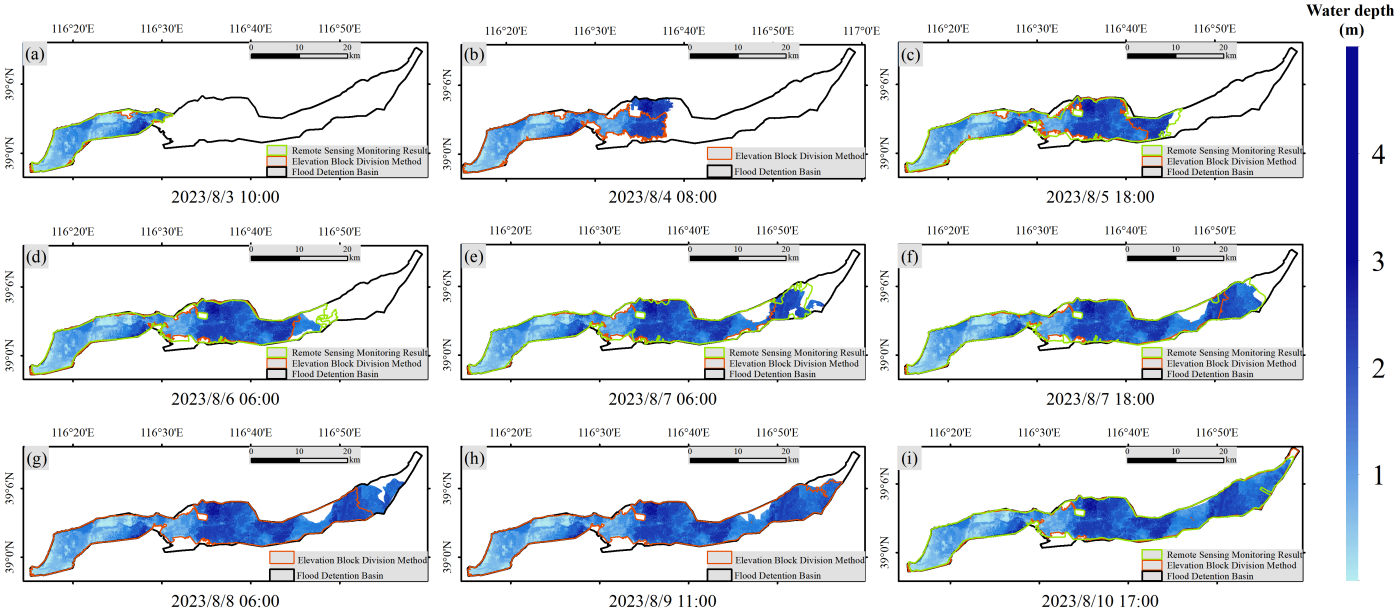


Figure 11. Comparison of Simulated Inundation Extent between TSLIC Clustering and elevation-based Partitioning method.

Comparative analysis of the simulation results shows that inundation areas derived from the elevation-based Partitioning method are generally smaller than those obtained using TSLIC. When compared with remote sensing observations, four simulation periods produced inundation extent errors greater than 10%, with the maximum error approaching 20%. In addition, the simulation errors show large temporal fluctuations. These errors mainly arise because the elevation-based Partitioning method cannot effectively represent the terrain characteristics of the Dongdian FSDB. The Dongdian area is dominated by flat terrain, and the elevation-based Partitioning method applies a fixed elevation interval of 0.2 m for terrain clustering. This results in a small number of terrain blocks with excessively large areas, which limits the ability to represent detailed flood spreading paths. The oversized terrain blocks significantly increase internal flow propagation time, which causes delayed inundation expansion in the simulation. As a result, the modeled inundation extent cannot respond in a timely manner to dynamic changes in flood inflow.

4.2.2. Comparison of Flood Evolution Methods

In the RS-CFPM model, flood propagation speed is estimated by combining velocities calculated using the Manning equation and velocities derived from remote sensing observations. The Manning equation requires three parameters: roughness coefficient n, hydraulic radius R, and slope S (Equation (6)). The Dongdian FSDB is characterized by flat terrain, with an average surface slope ranging from 1/6000 to 1/10,000. Based on terrain characteristics of the study area and related studies [11], roughness values were assigned as follows: 0.14 for cropland, 0.19 for residential areas, 0.18 for roads, 0.10 for forest land, 0.045 for grassland, and 0.04 for water bodies. In the RS-CFPM model, the computational units are superpixel-based terrain units, which can be approximated as rectangular in two dimensions. Because the average size of each terrain unit is much larger than floodwater depth, the flow cross-section can be simplified as a rectangle, and the hydraulic radius R is approximated by water depth. Flood propagation speed derived from remote sensing was

calculated using consecutive radar images. We first extracted the displacement of the water front between inundation extents in adjacent images. We then divided the displacement by the corresponding time interval to obtain the average propagation velocity V. The weighting coefficient λ was adjusted based on spatial distance from the flood diversion gate. Areas closer to the floodgate are more strongly influenced by inflow momentum during flood propagation. Therefore, a higher weight is assigned to the remote sensing-derived velocity V in these areas. As the distance from the floodgate increases, the influence of gate momentum gradually decreases. Flood expansion then becomes more controlled by terrain-driven overflow, and a higher weight is assigned to the velocity estimated from the Manning equation. The weighting factor λ changes continuously in space. It remains constant over time during the rising stage of the flood. This setting avoids introducing too many free parameters and helps maintain model stability for emergency applications. By adjusting these parameters, a spatial distribution of flow velocity was obtained, as shown in Figure 12, which shows that flood flow velocity in the Dongdian FSDB generally decreases from west to east. Areas with higher roughness, such as cropland and residential land, exhibit lower flow velocities. The average flow velocity is approximately 0.15 m/s in cropland and about 0.6 m/s in residential areas.

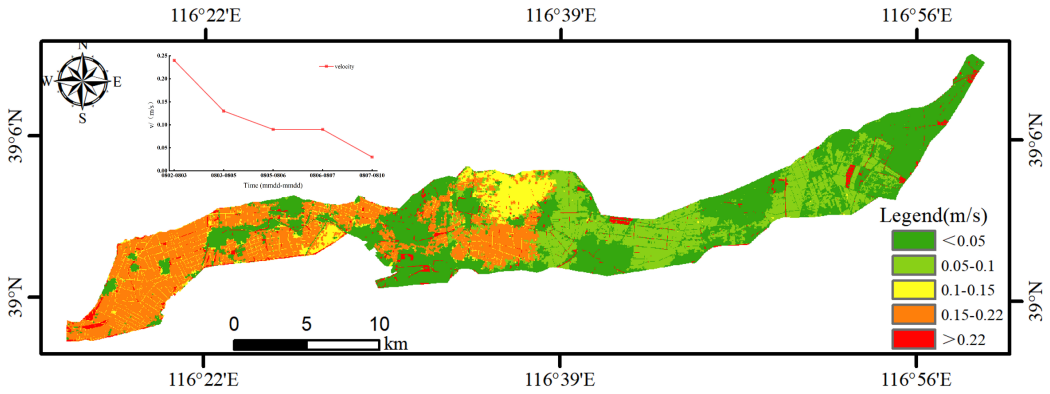


Figure 12. Spatial distribution of flow velocity in Dongdian FSDB

To evaluate the flood simulation performance of the RS-CFPM model, the TSLIC-based clustered terrain was used as a unified terrain input. Flood inundation processes in the Dongdian FSDB were simulated using both the RS-CFPM model and the Bathtub Model, and the dynamic changes in inundation extent were obtained. It should be noted that simulations were conducted only for time steps with available remote sensing images, as well as for 4, 8, and 9 August, and these results are presented as representative examples. Figure 13 provides a direct comparison of the inundation dynamics simulated by the two models.

Comparative analysis shows clear differences between the two simulation results during flood evolution. The Bathtub Model consistently produces larger inundation extents than the RS-CFPM model at all time steps. When compared with remote sensing observations, inundation extent errors from the Bathtub Model generally exceed 10%, with the maximum error exceeding 20%. At 06:00 on 6 August, the Bathtub Model simulation indicates that the Dongdian FSDB is almost completely inundated, whereas the RS-CFPM simulation shows full inundation occurring on 10 August (Figure 13d). The Dongdian FSDB is characterized by flat terrain and a relatively limited spatial scale. The main reason for inundation overestimation by the Bathtub Model is that it ignores the time required for floodwater to propagate over real terrain. In the Bathtub Model, any area with an elevation lower than the current water level is immediately classified as inundated, regardless of

whether the flood wave has actually reached that location. This assumption leads to a significant overestimation of inundation extent at the same time step.

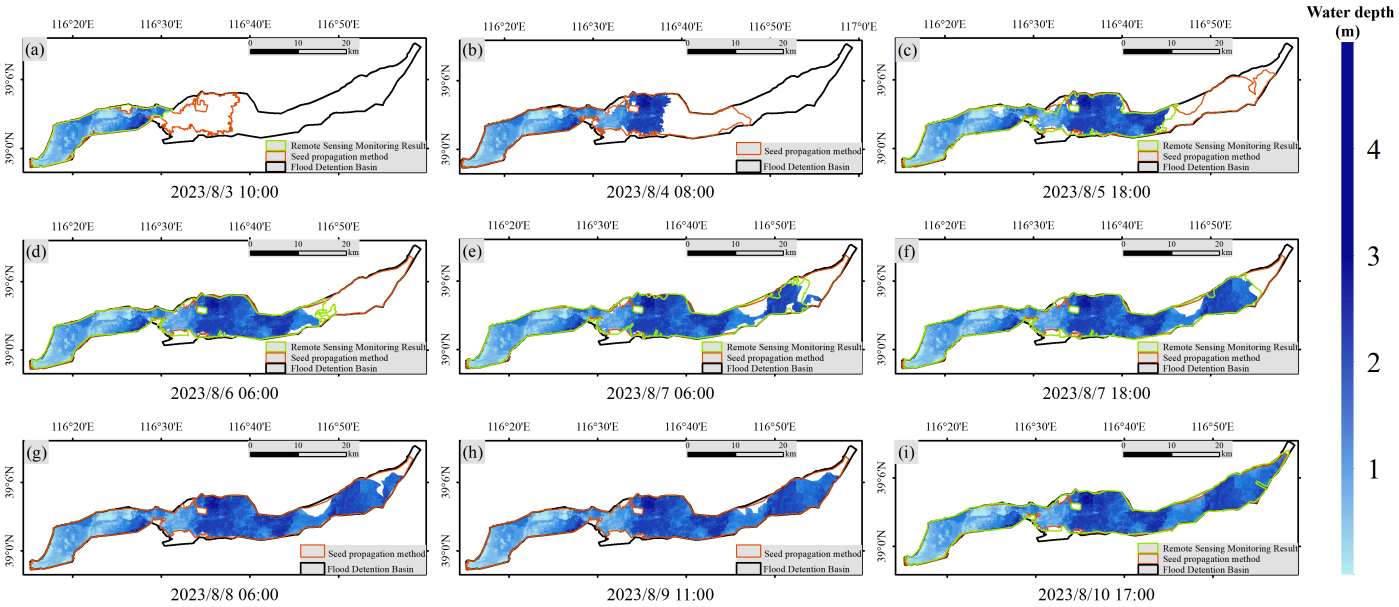


Figure 13. Comparison of Inundation Process between RS-CFPM and Bathtub Model.

5. Discussion

5.1. Performance and Mechanistic Interpretation of the RS-CFPM Model

Results from the Dongdian FSDB case indicate that the RS-CFPM model performs reliably in representing the spatiotemporal dynamics of flood evolution. The simulated inundation extent and water level show good agreement with radar remote sensing observations, with errors generally within 10%. Compared with the traditional Bathtub Model, RS-CFPM significantly reduces systematic overestimation during the early stage and rapid rising stage of flooding. This improvement is mainly due to the introduction of propagation time constraints.

Previous studies have shown that static or quasi-static inundation simulation methods often produce temporal distortion because they ignore the physical time required for flood propagation [24–26]. By coupling propagation delay constraints within a water balance framework, the RS-CFPM model improves temporal consistency of flood evolution while keeping computational cost relatively low. This result highlights the effectiveness of introducing key physical constraints into a simplified modeling framework.

When compared with physics-based hydrodynamic models [38], RS-CFPM adopts a simplified process representation but achieves comparable simulation accuracy in flat flood storage–detention basins, with errors below 10%. This suggests that, in areas with relatively flat terrain where flood expansion is mainly dominated by overbank spreading, a simplified model that combines terrain clustering with propagation constraints can achieve accuracy similar to hydrodynamic models at a much lower computational cost. This feature is especially valuable for emergency flood assessment.

In terms of computational efficiency, RS-CFPM achieves more than a 60% improvement compared with the Bathtub Model. In addition, compared with DEM block-based dynamic simulation methods [27,28], TSLIC-based terrain clustering generates spatially continuous and uniformly sized units, which avoids propagation delay caused by oversized terrain blocks. As a result, the model shows more stable and reliable performance in flat flood storage–detention basins.

5.2. Applicability and Limitations of the RS-CFPM Model

It should be noted that the RS-CFPM model is a simplified flood evolution simulation method designed for flood emergency response. The main goal of the model is to achieve rapid computation while maintaining reasonable accuracy. Therefore, the model uses simplified representations of some physical processes.

In this study, the model adopts a near-level water surface assumption within a water balance framework to estimate the average water level at each time step. This assumption is an idealized treatment from a strict hydrodynamic perspective. It is mainly suitable for areas with gentle terrain slope, weak water surface gradient, overflow-dominated flood expansion, and no long-term enclosed water-level zones. The Dongdian FSDB has a relatively flat terrain. Before flood diversion, the embankment was artificially breached to form openings, and flood expansion mainly occurred through overflow and bypass flow. At the regional scale, the water surface tends to behave as a quasi-static system. Therefore, the assumption is considered reasonable in this study. If this assumption is violated, the model may predict earlier inundation timing in distant areas, underestimate local water depth, or overestimate inundation extent in some regions. To reduce these effects, the model introduces a propagation time constraint. This mechanism limits errors caused by instantaneous uniform spreading. Under the constraint of total inflow volume, this assumption mainly affects inundation timing and local water depth distribution, while its influence on the final maximum inundation extent remains limited.

For flood propagation velocity, the model combines velocity estimated from the Manning equation with flood-front speed derived from remote sensing using a weighting factor λ. Changes in λ mainly affect the timing and spatial pattern of flood propagation. When λ increases, the propagation pattern becomes closer to the average speed observed from remote sensing, and velocity differences between regions decrease. When λ decreases, local terrain and roughness exert stronger control, and spatial differences in propagation increase. Therefore, λ can be regarded as a balance parameter between large-scale propagation characteristics and local overflow capacity. Under a constant total inflow volume, λ has limited influence on the final maximum inundation extent. Its main effect appears in the arrival time distribution during the rising stage of flooding.

Model results are also affected by DEM accuracy and parameter settings. In very flat areas, small vertical errors may lead to noticeable changes in horizontal inundation boundaries. Because this study targets emergency applications, systematic quantitative uncertainty propagation analysis was not conducted. Overall, DEM and parameter errors mainly affect local inundation boundaries and propagation timing, but they do not significantly change the overall inundation trend under the constraint of volume conservation. Future work can further quantify uncertainty propagation.

Overall, RS-CFPM lies between traditional static inundation models and full hydrodynamic models. The model introduces propagation time constraints and physically based flow velocity estimation to improve the physical consistency of flood evolution timing while maintaining low computational complexity. The method is suitable for rapid emergency decision support in plain flood storage and detention basins. However, its applicability in complex urban environments or strongly dynamic hydraulic conditions still requires further evaluation. Future studies may introduce multi-source data constraints and improved propagation parameterization for such environments.

6. Conclusions

To enable rapid and accurate simulation of flood inundation processes in flood storage–detention basins under emergency conditions, this study proposes a high-accuracy flood evolution simulation method that integrates terrain clustering with physical con-

straints. A high-resolution DEM with a spatial resolution of 2 m was constructed using GaoFen-7 remote sensing imagery and laser altimetry data. The DEM was clustered using the TSLIC algorithm, in which elevation values replace color information, and the clustered terrain was used as model input. Based on this terrain representation, the RS-CFPM model, which combines water balance with flow propagation constraints, was applied to dynamically simulate flood inundation processes in flood storage–detention basins. The proposed method was applied to the Dongdian FSDB, and the main conclusions are as follows:

(1) The simulated inundation extent shows good agreement with inundation maps derived from synchronous remote sensing images. The simulation accuracy is comparable to that of the hydrodynamic model reported by Wu et al. [38], with relative errors in inundation area and water level both below 10%. Compared with traditional seed-spreading methods, the proposed method achieves a computational efficiency improvement of over 60%, confirming its applicability in flood storage–detention basin scenarios.
(2) Compared with the traditional elevation-based Partitioning method, TSLIC-based terrain clustering significantly reduces inundation extent errors. The TSLIC-based results maintain errors below 10%; TSLIC can better identify micro-topographic features and generate compact and regular superpixel units, which avoids the fragmented and discontinuous regions produced by the traditional elevation-based Partitioning method.
(3) When compared with the Bathtub Model, the RS-CFPM model shows more stable and accurate simulation results; inundation extent errors produced by the RS-CFPM model remain below 10%. By incorporating water balance and flow propagation velocity constraints, the RS-CFPM model produces flood evolution results that are consistent with observed flood regulation processes.

Overall, this study proposes a flood inundation simulation method for flood storage–detention basins that achieves both high accuracy and high efficiency. By reducing data dimensionality through terrain clustering and introducing flow propagation delay and water level feedback mechanisms, the proposed method enables efficient and accurate simulation of flood evolution processes. The results demonstrate that the method can support flood regulation analysis and emergency decision-making in flood storage–detention basins.

Author Contributions: Conceptualization, X.Z., S.Y. and X.L.; methodology, X.Z., S.Y., Q.L. and X.L.; software, X.Z., Y.S. and X.L.; validation, X.Z., Q.L. and B.C.; formal analysis, X.Z., Q.L. and B.C.; investigation, X.Z., S.Y., Q.S. and M.Y.; resources, X.Z., Q.L. and B.C.; data curation, X.L. and Y.S.; writing—original draft preparation, X.Z.; writing—review and editing, X.Z., X.L. and Y.S.; visualization, X.Z., Q.L. and B.C.; supervision, Q.S., M.Y., X.L. and Y.S.; project administration, X.L. and Y.S.; funding acquisition, X.L. and Y.S. All authors have read and agreed to the published version of the manuscript.

Funding: This research was funded by National Key Research and Development Program of China under Grant (2024YFC3012301) and the Jing-Jin-Ji Regional Integrated Environmental Improvement–National Science and Technology Major Project (Grant No. 2025ZD1208305).

Data Availability Statement: The data presented in this study are available upon request from the corresponding author.

Acknowledgments: The authors thank the data providers for making the following data available: Remote sensing and altimetry data were accessed on the China Centre for Resources Satellite Data and Application (https://data.cresda.cn/).

Conflicts of Interest: Author Shifan Yuan was employed by the Power China Kunming Engineering Corporation Limited. The remaining authors declare that the research was conducted in the absence of any commercial or financial relationships that could be construed as a potential conflict of interest.

References

1. Rentschler, J.; Avner, P.; Marconcini, M.; Su, R.; Strano, E.; Vousdoukas, M.; Hallegatte, S. Global evidence of rapid urban growth in flood zones since 1985. *Nature* **2023**, *622*, 87–92. [CrossRef] [PubMed]
2. Qin, G.; Wang, S.; Wang, F.; Li, S.; Gu, X.; Chen, B.; Wang, X.; Wang, Z.; Hu, K.; Zhu, J. Rapid flood detection in global scene based on multimodal data collaboration. *Int. J. Digit. Earth* **2025**, *18*, 2554307. [CrossRef]
3. Li, C.; Tian, J.; Shen, R. Review on assessment of flood and waterlogging risk. *J. Catastrophol.* **2020**, *35*, 131–136.
4. Dang, P.; Zhu, J.; Dang, C.; Zhang, H. A method for assessing urban flood impacts by combining hydrodynamic models with entity semantic evolution. *Int. J. Digit. Earth* **2025**, *18*, 2515268. [CrossRef]
5. Paprotny, D.; Tilloy, A.; Treu, S.; Buch, A.; Vousdoukas, M.I.; Feyen, L.; Kreibich, H.; Merz, B.; Frieler, K.; Mengel, M. Attribution of flood impacts shows strong benefits of adaptation in Europe since 1950. *Sci. Adv.* **2025**, *11*, eadt7068. [CrossRef]
6. Duan, R.; Huang, G.; Zhou, X.; Lu, C.; Tian, C. Record-Breaking heavy rainfall around Henan Province in 2021 and future projection of extreme conditions under climate change. *J. Hydrol.* **2023**, *625*, 130102. [CrossRef]
7. Shu, Z.; Li, W.; Zhang, J.; Jin, J.; Xue, Q.; Wang, Y.; Wang, G. Historical Changes and Future Trends of Extreme Precipitation and High Temperature in China. *Strateg. Study Chin. Acad. Eng.* **2022**, *24*, 116–125. [CrossRef]
8. Du, H.; Zeng, S.; Zhang, Y.; Chen, Y.; Yang, L.; Xia, J. Climate change will lead to different over-threshold flood risks patterns of the riverside cities in the Yangtze River Basin. *J. Hydrol.* **2025**, *661*, 133664. [CrossRef]
9. Zhao, Z.; Huo, A.; Liu, Q.; Yang, L.; Luo, C.; Ahmed, A.; Elbeltagi, A. Assessment of urban inundation and prediction of combined flood disaster in the middle reaches of Yellow river basin under extreme precipitation. *J. Hydrol.* **2024**, *640*, 131707. [CrossRef]
10. Tang, Y.; Zhang, Y.; Zhang, G.; Li, S.; Gu, W.; Ou, M.; Zheng, Y. Study on the operation process of Dongdian Flood Detention and Storage Area in Haihe River Basin based on multi-source remote sensing images. *Eng. J. Wuhan Univ.* **2025**, *58*, 782–791+829.
11. Wu, B.; Ma, F.; Hu, S.; Zhang, L.; Zhao, Y.; Song, W.; He, B.; Liu, H.; Yu, H. Retrospective Analysis of Flood Propagation in the Dongdian Flood Storage-Detention Area During the '23·7' Extreme Flood Event in the Haihe River Basin. *Water Resour. Prot.* **2025**, *41*, 96–105.
12. Liao, S.; Wang, W.; Wang, C.; Ji, R.; Cui, A.; Chen, D.; Zhang, X.; Chen, N. Land Use and Land Cover Change Assessment and Predictions in Flood Detention Areas of Yangtze River Basin Based on AIF-HOM-PLUS Model. *Remote Sens.* **2025**, *17*, 1857. [CrossRef]
13. Amer, R. Machine Learning-Driven Rapid Flood Mapping for Tropical Storm Imelda Using Sentinel-1 SAR Imagery. *Remote Sens.* **2025**, *17*, 1869. [CrossRef]
14. Ben, P.; Li, J.; Yu, B.; Hu, Y. Discussion on the Mode of Using Flood Storage Area Based on the Combination of Extreme Value and Flood Volume. *J. China Hydrol.* **2021**, *41*, 28–34.
15. Shuihua, J.; Zhongfa, H.; Jinsong, H.; Ying, Z.; Xianhe, J. Flood evolution simulation in flood storage and detention area and evaluation methods for the dike-break losses. *J. Water Resour. Water Eng.* **2020**, *31*, 131–139+145.
16. Zhu, J.; Wang, Z.; Li, Y. Analysis of Groundwater Impact Characteristics of '23·7' Basin-wide Extraordinary Flood in Haihe River Basin. *Water Resour. Power* **2025**, *43*, 23–26.
17. Hao, S.; Wang, W.; Ma, Q.; Li, C.; Liu, C. Analysis on the Disaster Mechanism of the '8·12' Flash Flood in Liulin River Basin, Hubei Province. *J. Basic Sci. Eng.* **2024**, *32*, 133–144.
18. Saha, A.; Stelling, G.; Vuik, C. Modified Horton's infiltration model integrated with a Sub-Grid shallow water equation solver for High-Resolution flooding simulation. *J. Hydrol.* **2025**, *660*, 133326. [CrossRef]
19. Ding, Z.; Li, J.; Li, L. Method for flood submergence analysis based on GIS grid model. *J. Hydraul. Eng.* **2004**, *6*, 56–60+67.
20. Shen, Z.; Ding, Y.; Kong, Q. Application Study of Coupling Rainfall-runoff Modeling and Floodplain Inundation Mapping. *J. Geo-Inf. Sci.* **2021**, *23*, 1473–1483.
21. Ma, Q.; Li, Z.; Dong, F.; Zhang, K.; Yang, B.; Liu, C. Flood modeling developed for digital twin water-shed: A case study of '23·7' great flood assessment in Ziya River Basin. *J. Hydraul. Eng.* **2025**, *56*, 73–84.
22. Zhang, H.; Wu, W.; Hu, C.; Hu, C.; Li, M.; Hao, X.; Liu, S. A distributed hydrodynamic model for urban storm flood risk assessment. *J. Hydrol.* **2021**, *600*, 126513. [CrossRef]
23. Samadi, A.; Jafarzadegan, K.; Moradkhani, H. DEM-based pluvial flood inundation modeling at a metropolitan scale. *Environ. Model. Softw.* **2025**, *183*, 106226. [CrossRef]
24. Que, J.; Tan, J. Research of Flood Routing Process in the Downstream of the Reservoir Based on DEM. *Water Resour. Power* **2024**, *42*, 212–215.
25. Yang, A.; Song, S.; Wang, H.; Wu, D. Research and Application of Flood Inundation Analysis Algorithm Based on Digital Elevation Model. *Geomat. Spat. Inf. Technol.* **2023**, *46*, 44–47.
26. Wijaya, O.T.; Yang, T.H.; Hsu, H.M.; Gourbesville, P. A rapid flood inundation model for urban flood analyses. *MethodsX* **2023**, *10*, 102202. [CrossRef]
27. Wang, S.; Li, Y.; Liu, P.; Geng, Z.; Sun, X. Algorithm for Calculating Flood Submergence Range from DEM Data Based on Graph Traversal. *Remote Sens. Inf.* **2020**, *35*, 87–92.

28. Yu, C.; Hu, D.; Zhang, Y.; Cao, S.; Wang, S. Research and Application of Flood Dynamic Evolution Algorithm by DEM Spatial Partition. *Sci. Surv. Mapp.* **2020**, *45*, 181–189.
29. Teng, J.; Jakeman, A.J.; Vaze, J.; Croke, B.F.; Dutta, D.; Kim, S. Flood inundation modelling: A review of methods, recent advances and uncertainty analysis. *Environ. Model. Softw.* **2017**, *90*, 201–216. [CrossRef]
30. Jamali, B.; Bach, P.M.; Cunningham, L.; Deletic, A. A Cellular Automata fast flood evaluation (CA-ffé) model. *Water Resour. Res.* **2019**, *55*, 4936–4953.
31. Thrysøe, C.; Balstrøm, T.; Borup, M.; Löwe, R.; Jamali, B.; Arnbjerg-Nielsen, K. FloodStroem: A fast dynamic GIS-based urban flood and damage model. *J. Hydrol.* **2021**, *600*, 126521. [CrossRef]
32. Yu, H.; Li, C.; Liu, Z.; Zhou, S.; Guo, Y. Remote sensing image dehazing algorithm based on adaptive SLIC. *Natl. Remote Sens. Bull.* **2024**, *28*, 3158–3172.
33. Zhan, N.; Li, X.; Lu, J.; Xu, W. Water body information extraction by Sentinel -1 radar data based on SLIC. *Yangtze River* **2020**, *51*, 213–217+225.
34. Tong, H.; Tong, F.; Zhou, W.; Zhang, Y. Purifying SLIC superpixels to optimize superpixel-based classification of high spatial resolution remote sensing image. *Remote Sens.* **2019**, *11*, 2627. [CrossRef]
35. Wang, N.; Chen, F.; Yu, B.; Wang, L. A strategy of parallel slic superpixels for handling large-scale images over apache spark. *Remote Sens.* **2022**, *14*, 1568.
36. Zhao, W.; Liu, Y.; Wu, X.; Jiao, P.; Zhang, X. Accuracy Verification of the Scale of 1:10,000 stereo Mapping Based on GaoFen-7 Satellite Imagery. *Acta Geod. Cartogr. Sin.* **2022**, *47*, 165–171+180.
37. He, F.; Mahmud, M.P.; Kouzani, A.Z.; Anwar, A.; Jiang, F.; Ling, S.H. An improved SLIC algorithm for segmentation of microscopic cell images. *Biomed. Signal Process. Control* **2022**, *73*, 103464. [CrossRef]
38. Liu, M.; Jin, S.; Gu, C.; Li, J.; Li, S.; Liu, L. Chinese Satellite-based Flood Mapping and Damage Assessment in Dongdian Flood Detention Basin, China. *J. Resour. Ecol.* **2024**, *15*, 1344–1357. [CrossRef]
39. Wu, B.; Yu, W.; Ma, F.; Yu, H.; Mu, J.; Chai, F.; Li, M.; Song, W. Simulation and forecasting of flood evolution in Dongdian storage-detention area during Haihe "23 · 7" basin-wide extreme flood. *China Flood Drought Manag.* **2023**, *33*, 37–42+57.
40. Li, G.; Tang, X.; Chen, J.; Yao, J.; Liu, Z.; Gao, X.; Zuo, Z.; Zhou, X. Processing and preliminary accuracy validation of the GF-7 satellite laser altimetry data. *Acta Geod. Cartogr. Sin.* **2021**, *50*, 1338–1348.
41. Tang, X.; Liu, C.; Zhang, H.; Wang, X.; Li, G.; Mo, F.; Li, F. GF-7 Satellite Stereo Images Block Adjustment Assisted with Laser Altimetry Data. *Geomat. Inf. Sci. Wuhan Univ.* **2021**, *46*, 1423–1430.

Disclaimer/Publisher's Note: The statements, opinions and data contained in all publications are solely those of the individual author(s) and contributor(s) and not of MDPI and/or the editor(s). MDPI and/or the editor(s) disclaim responsibility for any injury to people or property resulting from any ideas, methods, instructions or products referred to in the content.